CHINESE OPTICS LETTERS

Vol. 22, No. 2 | February 2024

High-resolution portable lens-free on-chip microscopy with RGB LED via pinhole array

Qinhua Wang (王钦骅)[1], Jianshe Ma (马建设)[1], Liangcai Cao (曹良才)[2], and Ping Su (苏 萍)[1*]

[1] Tsinghua Shenzhen International Graduate School, Tsinghua University, Shenzhen 518055, China

[2] Department of Precision Instrument, Tsinghua University, Beijing 100084, China

*Corresponding author: su.ping@sz.tsinghua.edu.cn

Received February 7, 2023 | Accepted September 20, 2023 | Posted Online February 20, 2024

Lens-free on-chip microscopy with RGB LEDs (LFOCM-RGB) provides a portable, cost-effective, and high-throughput imaging tool for resource-limited environments. However, the weak coherence of LEDs limits the high-resolution imaging, and the luminous surfaces of the LED chips on the RGB LED do not overlap, making the coherence-enhanced executions tend to undermine the portable and cost-effective implementation. Here, we propose a specially designed pinhole array to enhance coherence in a portable and cost-effective implementation. It modulates the three-color beams from the RGB LED separately so that the three-color beams effectively overlap on the sample plane while reducing the effective light-emitting area for better spatial coherence. The separate modulation of the spatial coherence allows the temporal coherence to be modulated separately by single spectral filters rather than by expensive triple spectral filters. Based on the pinhole array, the LFOCM-RGB simply and effectively realizes the high-resolution imaging in a portable and cost-effective implementation, offering much flexibility for various applications in resource-limited environments.

Keywords: lens-free on-chip microscopy; LED; phase retrieval; pinhole array.

DOI: 10.3788/COL202422.021101

1. Introduction

In recent years, the emergence and development of lens-free on-chip microscopy (LFOCM) provides a potential solution to simultaneously realize high-resolution and large field-of-view (FOV) on a portable and cost-effective system, which is useful as a point-of-care testing tool for telemedicine applications, point-of-care diagnostics, and analysis of natural water samples in resource-limited environments[1–7]. Using the RGB LED as the light source of the LFOCM (LFOCM-RGB) can conveniently obtain the three-color holograms without complicated optical assembly and time-consuming mechanical operations, effectively providing two options for microscopic imaging applications. One option is to reconstruct the three-color holograms separately by single-intensity phase retrieval and digitally superimpose the three-color reconstructions to realize color imaging[8,9], which provides time-lapse imaging results of dynamic specimens. The other option is to fuse the three-color holograms by using multi-intensity phase retrieval[10–13] to effectively eliminate the twin-image caused by phase loss, which is suitable to perform precise quantitative phase retrieval for a static specimen[14–16].

Despite the fact that the LFOCM-RGB has the unique potential to provide a portable, cost-effective, stable, and high-throughput imaging tool, the large light-emitting area and broad emission spectrum of the RGB LED result in weak spatial and temporal coherence of the three-color beams, limiting the imaging resolution[4,17]. As the luminous surfaces of the three LED chips on the RGB LED do not overlap, the LFOCM-RGB poses challenges for coherence improvement that should be addressed with particular care. To overcome this problem, conventional methods rely on additional optical accessories (e.g., a fiber-optic cable[18] or a pinhole coupled with a diffuser[15,16]) or increasing the distance from the light source to the sample[8,9] to reduce the effective light-emitting area for better spatial coherence. The above methods require the expensive triple spectral filter to reduce the emission spectrum for better temporal coherence. This will undermine the implementation of a portable and cost-effective system, making it difficult for LFOCM-RGB to be portable and with high-resolution at the same time.

In this Letter, we propose a specially designed pinhole array to enhance the coherence in a portable and cost-effective implementation. It modulates the three-color beams from the RGB LED separately so that the three-color beams effectively overlap on the sample plane while enhancing the spatial and temporal coherence to realize high-resolution imaging on a portable and cost-effective LFOCM-RGB.

2. Methods and Experiment

There is no numerical aperture (NA) of the objective lens to limit the resolution in LFOCM. Therefore, assuming that the image sensor could have arbitrarily small pixels and arbitrarily large photosensitive areas, the spatial and temporal coherence properties of the light source independently determine the resolution[4,17]. Spatial coherence is primarily influenced by the effective light-emitting area, which is determined by the size of the light source and the source-to-sample distance, while the temporal coherence is primarily determined by the spectral bandwidth of the light source. Considering the large light-emitting area and broad emission spectrum of LEDs, LFOCM using LEDs as the light source will be able to realize high-resolution lens-free imaging if the effective light-emitting area of the LEDs can be reduced to improve spatial coherence and the spectral bandwidth can be reduced to improve temporal coherence. Portability is a goal for the effective use of LFOCM in resource-limited environments, so it is a topic of interest to improve the coherence of the light source in a simple and cost-effective way without increasing the size of the LFOCM. Compared to increasing the distance from the light source to the sample or coupling the LED to a fiber-optic cable[18], coupling the LED directly to a pinhole to reduce the effective light-emitting area for better spatial coherence is cost-effective and simple.

The pinhole reduces the effective light-emitting area of the LED, while imaging the luminous surface of the LED chip onto the sample plane to illuminate the sample. However, the luminous surfaces of the three LED chips on the RGB LED do not overlap, and the spots generated by the three-color beams passing through a pinhole do not overlap each other when a pinhole is coupled behind the RGB LED, as shown in Fig. 1(a). The LFOCM-RGB realizes color imaging or quantitative imaging only for the region co-illuminated by the three-color beams.

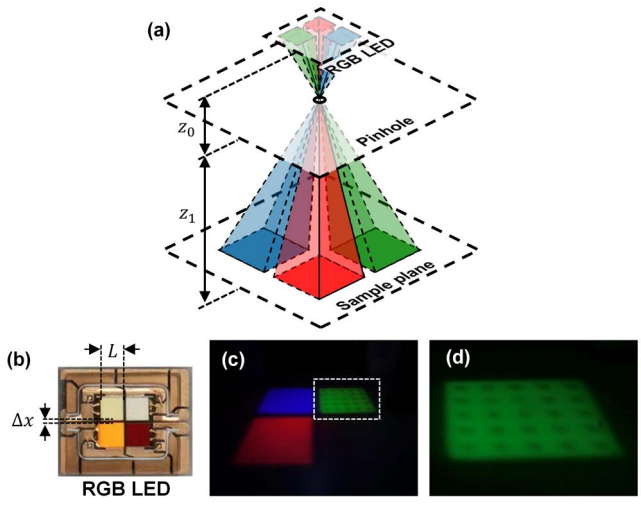

Fig. 1. (a) The illumination schematic of the RGB LED filtered by a pinhole. (b) The photograph of the RGB LED. (c) The spots generated by three-color beams on the sample plane. (d) The enlarged region corresponding to the white boxed area in (c).

Therefore, by coupling a pinhole behind the RGB LED, the superimposition or fusion of the three-color holograms is limited or even fails. We coupled a pinhole of 100 μm diameter below an RGB LED [OSRAM LE RTDCY S2WN, with dominant wavelengths of 625 nm, 525 nm, and 453 nm. The LED chips are squares with the side length L of 1 mm and the spacing Δx of 0.1 mm, as shown in Fig. 1(b)] to build a partially coherent light source for experimental verification. We used the USB interface of the laptop to power the RGB LED (less than 2.5 W). The distance from the RGB LED to the pinhole is 3 mm (z_0), and the distance from the pinhole to the sample plane is 50 mm (z_1). As shown in Figs. 1(c) and 1(d), when all three colors of the LED chips were turned on, the pinhole imaged the luminous surface of the LED chips on the whiteboard, where the images of the electrode lattices and edges on the LED were clearly visible. And the spots generated by the three-color beams on the whiteboard did not overlap.

To overcome this limitation, it has been proposed to place a diffuser between the pinhole and the RGB LED[15,16]. The diffuser scatters the incident three-color beams to increase the area of the luminous surfaces without affecting the relative position of the three-color spots formed on the pinhole, making the three-color beams overlap before passing through the pinhole. Therefore, the three-color spots on the sample plane will coincide into a white spot where the color imaging or quantitative imaging is available, as shown in Fig. 2(a). The size of the region co-illuminated by the three-color beams is primarily determined by the grit of the diffuser and the ratio (k) between the distance from the RGB LED to the pinhole array (z_0) and the distance from the pinhole to the sample plane (z_1). Without changing the distance from the RGB LED to the sample plane in Fig. 1 (53 mm), we inserted a single-sided grit-polished diffuser (2-mm thick) between the pinhole and the RGB LED.

As shown in Figs. 2(b1)–2(b3), the diffuser made the rectangle spots turn into circle spots, and the inherent thickness of the diffuser kept the pinhole away from the RGB LED, making the three-color spots smaller than the spots in Fig. 1(c). It also revealed that a coarser grit diffuser generated a larger circular spot (yellow dashed box). We turned on the red, green, and blue LED chips sequentially to obtain the size and position of the three-color spots. Based on the position and size of the obtained three-color spots, we circled the region co-illuminated by the three-color beams (white dashed box) and overlapped the white dashed box with the three-color spots co-illuminated by the three-color beams, as shown in Figs. 2(c1)–2(c3).

A more portable implementation on the LFOCM-RGB means that the distance from the RGB LED to the sample plane is smaller, and the inherent thickness of the diffuser keeps the pinhole away from the RGB LEDs, resulting in a smaller spot area on the sample plane. Therefore, a coarser grit diffuser is required to maintain the co-illuminated region, which includes the photosensitive area of the image sensor, to ensure the maximum FOV. However, the coarser grit diffuser will significantly reduce the illumination power on the sample, resulting in a poor signal-to-noise ratio (SNR) and making it difficult to couple the RGB LED to a smaller pinhole for better spatial coherence. At the

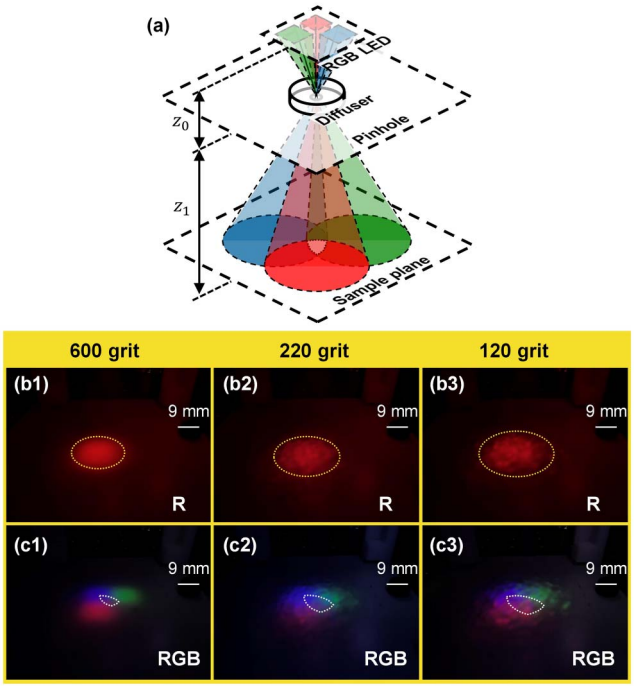

Fig. 2. (a) The illumination schematic of the RGB LED filtered by a pinhole and a diffuser. (b) The red spots obtained when the diffuser is 120 grit (b1), 220 grit (b2), and 600 grit (b3), respectively, and the yellow dashed boxes are the region illuminated by the red beam. (c) The three-color spots obtained when the diffuser is 120 grit (c1), 220 grit (c2), and 600 grit (c3), and the white dashed boxes are the region co-illuminated by the three-color beams.

same time, this method requires an expensive triple spectral filter to reduce the emission spectrum for better temporal coherence, which will increase the cost of LFOCM.

Compared with the diffuser, the proposed pinhole array can simply and efficiently generate co-illuminated areas on the sample plane while reducing the effective luminous surface size of the LED chips. The pinhole array sets up the same number of pinholes as the LED chips on the RGB LED, and these pinholes, respectively, image the luminous surfaces of different LED chips on the sample plane, as shown in Fig. 3(a). The relative position of the pinhole and the corresponding LED chip determines the position of the spot on the sample plane. Therefore, the pinhole array can effectively overlap the three-color spots by modulating the relative position of the pinhole and the corresponding LED chip. We designed the pinhole array based on the position of the LED chips encapsulated on the substrate in Fig. 1(b). According to the principle of pinhole imaging, assuming that each pinhole is a transparent point, the position of the region co-illuminated by the three-color beams is primarily determined by the relative position between the center of the pinhole array and the center of the RGB LED. The size of the region co-illuminated by the three-color beams (S) is influenced primarily by the pitch of the pinholes (Δd) and the ratio (k) between the distance from the RGB LED to the pinhole array (z_0) and the distance from the pinhole array to the sample plane (z_1). The relationship is given by

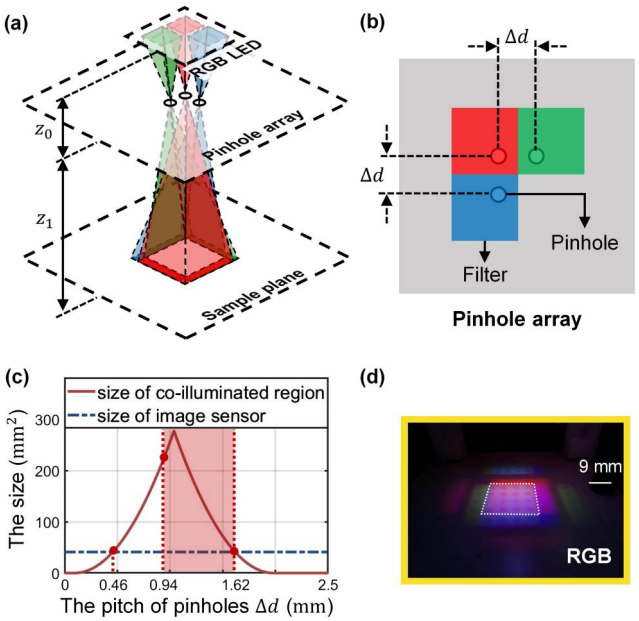

Fig. 3. (a) The illumination schematic of the RGB LED filtered by a pinhole array. (b) The schematic diagram of the pinhole array. (c) The effect of the pitch of pinholes (Δd) on the size of the region co-illuminated by the three-color beams, and the red region is the valid pitch of the pinholes. (d) The spot of the RGB LED on the sample plane with the pinhole array.

$$S=\begin{cases}\left(\dfrac{2L+\Delta x-\Delta d}{k}-\Delta d\right)^2, & \dfrac{L+\Delta x}{1+k}<\Delta d\le\dfrac{2L+\Delta x}{1+k}\\ \left(\dfrac{\Delta d-\Delta x}{k}+\Delta d\right)^2, & \dfrac{\Delta x}{1+k}<\Delta d\le\dfrac{L+\Delta x}{1+k}\\ 0, & \text{else}\end{cases},\tag{1}$$

where L denotes the side length of the LED chip and Δx denotes the spacing between the LED chips. We performed a theoretical calculation about the size of the region co-illuminated by the three-color beams based on the configuration in Fig. 1. As shown in Fig. 3(c), the size of the co-illuminated region is larger than the photosensitive size of the image sensor (Sony IMX226, 4072 × 3046, pixel size 1.85 μm) in our system when the pitch of the pinholes (Δd) is from 0.46 mm to 1.62 mm.

However, the spots generated by a single LED chip through different pinholes will overlap when the pitch of the pinholes (Δd) is less than $L/(1+k)$, resulting in the signal crosstalk between different pinholes. Therefore, the valid pitch of the pinholes (Δd) is from 0.94 mm to 1.62 mm, as shown in Fig. 3(c). We set the pinhole pitch (Δd) to 1.25 mm and the pinhole size to 100 μm and obtained the pinhole array by laser machining. As shown in the Fig. 3(d), the three-color spots on the sample plane effectively overlapped with the help of the pinhole array. Without changing the distance from the RGB LED to the sample plane, the size of the white spot obtained by the pinhole array was significantly larger than the size of the white spot obtained by the 120-grit diffuser shown in Fig. 2(c3). Since there is no loss

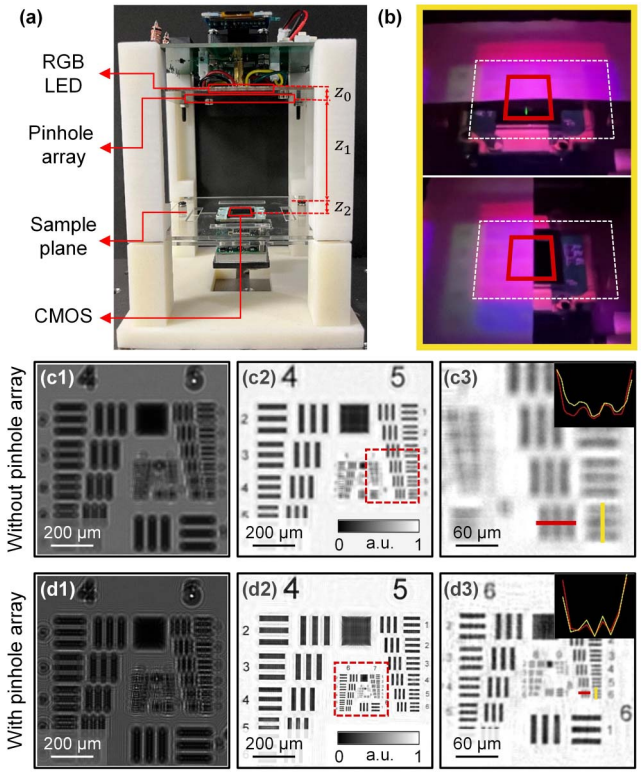

Fig. 4. (a) Schematic diagram of the LFOCM-RGB. (b) Three-color spots on the CMOS obtained with pinhole array. Raw hologram captured at the red light without the pinhole array (c1) and with the pinhole array (c2), and their amplitude distributions reconstructed by multi-wavelength phase retrieval in (c2) and (d2). (c3), (d3) The enlarged regions corresponding to the red boxed areas in (c2), (d2) and the amplitude values along the yellow and red lines.

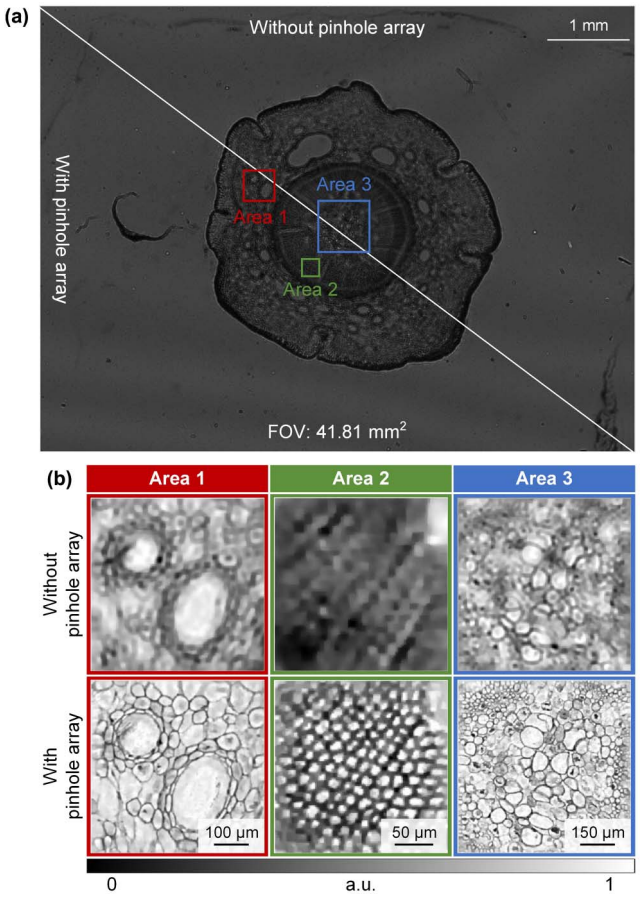

Fig. 5. Experimental result of pine stem. (a) The raw hologram captured at the red light without the pinhole array and with the pinhole array. (b) The amplitude distributions reconstructed by multi-wavelength phase retrieval corresponding to Area 1, Area 2, and Area 3 without the pinhole array and with the pinhole array.

of illumination power from the additional optical accessories, smaller pinholes can be used to realize better spatial coherence. At the same time, the separate modulation of the spatial coherence via three pinholes allows the temporal coherence of the three-color beams to be modulated separately by inserting three single spectral filters under the corresponding pinholes, instead of using an expensive triple spectral filter, as shown in the Fig. 3(b).

To the verify the resolution enhancement of the proposed pinhole array, we took a standard positive 1951 USAF resolution target as the sample and reconstructed the captured holograms by using the multi-wavelength phase retrieval algorithm[19] to eliminate twin-image. We continued to use the above configuration of the light source ($z_0 \approx 3$ mm and $z_1 \approx 50$ mm) and coupled the board-level CMOS sensor (Sony IMX226) to capture the three monochrome holograms in three measurements, as shown in Fig. 4(a). The sample-to-sensor distance (z_2) is 1 mm, and the FOV has the same size as the photosensitive area of the CMOS sensor, which is 41.81 mm^2. As shown in Fig. 4(b), the pinhole array effectively coincided with the three-color spots into a white spot (white dashed box), which is much larger than the photosensitive area of the image sensor (red solid box). Figure 4(c1) shows the raw hologram captured at the red light when the three-color beams propagated 50 mm to directly illuminate the sample. The large effective light-emitting area of the RGB LED resulted in weak spatial coherence, so the interference fringes on the hologram were not obvious, and the reconstructed amplitude distribution suggested that the half-pitch resolution reached only 8.77 μm (Group 5, Element 7) as shown in Figs. 4(c2) and 4(c3). In contrast, with the help of the pinhole array, there were clearer interference fringes on the hologram [Fig. 4(d1)] because the effective light-emitting area of the RGB LED was reduced to realize better spatial coherence, and the half-pitch resolution was enhanced to 2.2 μm (Group 7, Element 6), as shown in Figs. 4(d2) and 4(d3).

To further illustrate the applications of the pinhole array, we reconstructed the cross section of the pine stem without the pinhole array and with the pinhole array. As shown in Fig. 5, compared to the direct illumination of the sample using the three-color beams, we successfully identified the cytoarchitectural details about the resin ducts (Area 1), secondary xylem (Area 2), and pith (Area 3) of pine stem with the help of the proposed pinhole array.

3. Conclusion

To conclude, we proposed a specially designed pinhole array for LFOCM-RGB. The pinhole array has three pinholes, each of which images the luminous surfaces of the three chips on the RGB LED, respectively, so that the three-color beams effectively overlap on the sample plane while reducing the effective light-emitting area for better spatial coherence. At the same time, the separate modulation of spatial coherence via three pinholes allows the temporal coherence to be modulated separately by three single spectral filters, instead of using an expensive triple spectral filter. Based on the pinhole array, the LFOCM-RGB simply and effectively realizes high-resolution and wide-field imaging in a portable and cost-effective implementation, offering much flexibility for various applications in resource-limited environments.

Acknowledgements

This work was supported by the Shenzhen Key Basic Program (No. JCYJ20200109143031287) and the Shenzhen General Basic Program (No. WDZC20220816110140002).

References

1. A. Ozcan and U. Demirci, "Ultra wide-field lens-free monitoring of cells on-chip," Lab Chip **8**, 98 (2008).
2. G. Zheng, S. A. Lee, Y. Antebi, *et al.*, "The ePetri dish, an on-chip cell imaging platform based on subpixel perspective sweeping microscopy (SPSM)," Proc. Natl. Acad. Sci. U.S.A. **108**, 16889 (2011).
3. A. Greenbaum, Y. Zhang, A. Feizi, *et al.*, "Wide-field computational imaging of pathology slides using lens-free on-chip microscopy," Sci. Transl. Med. **6**, 267 (2014).
4. A. Ozcan and E. McLeod, "Lensless imaging and sensing," Annu. Rev. Biomed. Eng. **18**, 77 (2016).
5. Y. Gao and L. Cao, "High-fidelity pixel-super-resolved complex field reconstruction via adaptive smoothing," Opt. Lett. **45**, 6807 (2020).
6. Y. Gao and L. Cao, "Generalized optimization framework for pixel super-resolution imaging in digital holography," Opt. Express **29**, 28805 (2021).
7. Y. Gao, F. Yang, and L. Cao, "Pixel super-resolution phase retrieval for lensless on-chip microscopy via accelerated Wirtinger flow," Cells **11**, 1999 (2022).
8. Z. Göröcs, M. Tamamitsu, V. Bianco, *et al.*, "A deep learning-enabled portable imaging flow cytometer for cost-effective, high-throughput, and label-free analysis of natural water samples," Light Sci. Appl. **7**, 66 (2018).
9. Z. Göröcs, D. Baum, F. Song, *et al.*, "Label-free detection of *Giardia lamblia* cysts using a deep learning-enabled portable imaging flow cytometer," Lab Chip **20**, 4404 (2020).
10. P. Bao, F. Zhang, G. Pedrini, *et al.*, "Phase retrieval using multiple illumination wavelengths," Opt. Lett. **33**, 309 (2008).
11. D. W. E. Noom, K. S. E. Eikema, and S. Witte, "Lensless phase contrast microscopy based on multiwavelength Fresnel diffraction," Opt. Lett. **39**, 193 (2014).
12. X. Wu, J. Sun, J. Zhang, *et al.*, "Wavelength-scanning lensfree on-chip microscopy for wide-field pixel-super-resolved quantitative phase imaging," Opt. Lett. **46**, 2023 (2021).
13. Y. Gao and L. Cao, "Projected refractive index framework for multi-wavelength phase retrieval," Opt. Lett. **47**, 5965 (2022).
14. C. Zuo, J. Sun, J. Zhang, *et al.*, "Lensless phase microscopy and diffraction tomography with multi-angle and multi-wavelength illuminations using a LED matrix," Opt. Express **23**, 14314 (2015).
15. C. Allier, S. Morel, R. Vincent, *et al.*, "Imaging of dense cell cultures by multi-wavelength lens-free video microscopy," Cytometry **91**, 433 (2017).
16. L. Herve, O. Cioni, P. Blandin, *et al.*, "Multispectral total-variation reconstruction applied to lens-free microscopy," Biomed. Opt. Express **9**, 5828 (2018).
17. J. Zhang, J. Sun, Q. Chen, *et al.*, "Resolution analysis in a lens-free on-chip digital holographic microscope," IEEE Trans. Comput. Imaging **6**, 697 (2020).
18. W. Bishara, U. Sikora, O. Mudanyali, *et al.*, "Holographic pixel super-resolution in portable lensless on-chip microscopy using a fiber-optic array," Lab Chip **11**, 1276 (2011).
19. Q. Wang, J. Ma, and P. Su, "A multi-wavelength phase retrieval with multi-strategy for lensfree on-chip holography," Front. Photon. **3**, 865666 (2022).